Biomass Conversion and Biorefinery
https://doi.org/10.1007/s13399-023-04126-8

ORIGINAL ARTICLE

Antimicrobial and anticancer activities of biosynthesized bimetallic silver-zinc oxide nanoparticles (Ag-ZnO NPs) using pomegranate peel extract

Amr H. Hashem[1] · **Gharieb S. El-Sayyad**[2,3,4]

Received: 18 January 2023 / Revised: 7 March 2023 / Accepted: 12 March 2023

Abstract

In the last two decades, nanomaterials have received much attention for the treatment of multidrug-resistant microbes that threaten human health. In the current study, the novelty and scientific significance concentrated on the biogenic synthesis of bimetallic silver-zinc oxide nanoparticles (Ag-ZnO NPs) using pomegranate peel extract (PPE) for the first time. The new constructed bimetallic Ag-ZnO NPs possessed the synergistic activity at a low concentration to avoid toxicity and elevate the superior potential. UV-Vis. characterization illustrated that Ag-ZnO NPs were small in size (15.8 nm), which was observed at 395.0 nm. The SEM image of Ag-ZnO NPs, incorporated with PPE, exhibited uniform Ag-ZnO NP surfaces with a clear surface appearance. It can be detected that Ag-ZnO NPs were isolated typically as a rounded particle across the PPE, which showed as brilliant NPs combined and stabilized with the prepared PPE. Results also revealed that Ag-ZnO NPs exhibited potential antibacterial activity toward *Escherichia coli*, *Pseudomonas aeruginosa*, *Bacillus subtilis*, *Staphylococcus aureus*, and *Enterococcus faecalis* where minimum inhibitory concentrations (MICs) were 62.5, 125, 15.62, 62.5, and 250 µg/ml. Likewise, Ag-ZnO NPs appeared antifungal activity against *Candida albicans*, *Cryptococcus neoformans*, *Aspergillus fumigatus*, and *Aspergillus brasiliensis*, where MICs were 7.81, 31.25, 125, and 62.5 µg/ml, respectively. Moreover, Ag-ZnO NPs exhibited anticancer activities against MCF7 and Caco2, where IC_{50} was 104.9 and 52.4 µg/ml, respectively. Additionally, these concentrations are safe in use where results of cytotoxicity on Vero normal cell line confirmed that IC_{50} was 155.1 µg/ml. Overall, bimetallic Ag-ZnO NPs were for the first time, successfully biosynthesized using PPE; also, they had a promising antibacterial, antifungal, and anticancer activities.

Keywords Bimetallic nanoparticles · Antimicrobial activity · Cytotoxicity estimation · Pomegranate peel extract · Biomass

Abbreviations

Ag-ZnO NPs	Silver-zinc oxide nanoparticles
PPE	Pomegranate peel extract
UV–Vis.	Ultraviolet–visible
SEM	Scanning electron microscope
DLS	Dynamic light scattering
HR-TEM	High-resolution transmission electron microscope
XRD	X-ray diffraction
EDX	Energy dispersive X-Ray
FTIR	Fourier transform infrared
MICs	Minimum inhibitory concentrations
Caco2	Cancer coli-2
MCF7	Michigan cancer foundation-7
HeLa	Human cervical cancerous cells
HTC 116	Colorectal carcinoma
A 549	Adenocarcinomic human alveolar basal epithelial cells
IC50	Half-maximal inhibitory concentration
ATCC	American type culture collection
CFU	Colony-forming unit

✉ Gharieb S. El-Sayyad
Gharieb.Elsayyad@acu.edu.eg; Gharieb.Elsayyad@gu.edu.eg

[1] Botany and Microbiology Department, Faculty of Science, Al-Azhar University, Nasr City 11884, Cairo, Egypt

[2] Department of Microbiology and Immunology, Faculty of Pharmacy, Ahram Canadian University (ACU), Giza, Egypt

[3] Department of Microbiology and Immunology, Faculty of Pharmacy, Galala University, New Galala City, Suez, Egypt

[4] Drug Microbiology Lab., Drug Radiation Research Department, National Center for Radiation Research and Technology (NCRRT), Egyptian Atomic Energy Authority (EAEA), Cairo, Egypt

Published online: 06 April 2023

MTT	3-(4, 5-Dimethylthiazol-2-yl)-2, 5-diphenyl-2H-tetrazolium bromide
O.D.	Optical density
SPR	Surface plasmon resonance
PDI	Polydispersity index
JCPDS	Joint committee on powder diffraction standards
WH	Williamson-Hall

1 Introduction

Cancer is considered one of the most diseases which affect human health worldwide [1]. Chemotherapy is the common route for treating cancer due to its potential efficacy; however, it causes dangerous side effects such as hair loss, feeling tired most of the time, a sore mouth, and dry, sore, or itchy skin. Recently, some anticancer agents do not give high efficacy. Moreover, the abuse of antibiotics led to the development of multidrug-resistant bacteria around the world [2–4]. Thus, discovering new compounds that have antimicrobial and anticancer activities is highly needed.

Nanotechnology and nanomaterials have attracted the attention of most researchers in different fields such as medical, pharmaceutical, agricultural, environmental, and industrial fields [5–10]. Nanomaterials are frequently synthesized using chemical and physical methods. Although these methods have high efficacy, they are expensive and toxic to the environment [11]. Recently, plants, algae, fungi, and bacteria have been used as biological methods for the biosynthesis of nano-metals [12–20]. Ag NPs and ZnO NPs have been widely used in a variety of fields, including environmental, biomedical, and pharmaceutical applications. Studies have shown that shape and size of Ag NPs and ZnO NPs have a major impact on their electromagnetic, optical, and catalytic characteristics [21, 22]. Various morphologies, including discs, rods, wires, prisms, and spheres, of these NPs, have been produced in numerous research. Tetrahedrons, cubes, decahedrons, and pentagons are a few examples of certain shapes that have been successfully synthesized [23].

The biogenic synthesis of bimetallic Ag-ZnO NPs has been conducted in the literature. For instance, Sohrabnezhad et al. [24] synthesized Ag-ZnO NPs using *Urtica dioica* leaf extract for increasing the photocatalytic activity of Ag-ZnO NPs for dye removal. Additionally, Khatami et al. [25] utilize the extract of *Prosophis fracta* and coffee for the successful formation of Ag-ZnO NPs. The synthesized bimetallic NPs are also promising antibacterial agents against *Acinetobacter baumannii* and *Pseudomonas aeruginosa*. Furthermore, a recent report conducted a facile green synthesis route for Ag-ZnO nanocomposite synthesis using potato residue by simple and cost-effective combustion route [26]. The photocatalytic degradation of methylene blue (MB) dye was also investigated. Finally, Noohpisheh et al. [27] synthesized Ag-ZnO nanocomposites using *Trigonella foenum-graecum* leaf extract and investigated their antibacterial, antifungal, antioxidant, and photocatalytic properties.

Previous studies [28–31] used different kinds of peel for the biosynthesis of metal nanoparticles, but in this study, pomegranate peel was used due to its availability in the environment which causes many problems such as agro-wastes. The chemical constituents of the peel of pomegranate can help in the successful formation of stable bimetallic NPs. Regarding the biosynthesis of different NPs using the PPE, Hashem et al. [19] synthesized Se NPs using PPE in high concentration and narrow nano-size. The synthesized Se NPs possessed high activity which is simply used as antimicrobial, and antioxidant agents, in addition to their roles in biocompatibility and hemocompatibility.

This research aims to discuss one of the green ways for bimetallic Ag-ZnO NPs synthesis as well as their characterization and their biological activity as antimicrobial and anticancer agents. Due to the significant growth that has occurred in nanotechnology, various chemical, physical, and biological approaches have been created for generating Ag-ZnO NPs. To this end, the goal of this research was to use PPE extract to prepare bimetallic Ag-ZnO NPs as an eco-friendly and cost-effective method and to evaluate their ability to inhibit pathogenic bacteria and fungi, in addition to their anticancer potential.

2 Materials and methods

2.1 Chemicals and reagents

Media ingredients and components were purchased from Hi-Media and Difco. Chemicals such as silver nitrate, zinc nitrate, and other reagents (used in the following examinations) were obtained at the analytical standard grade from Sigma-Aldrich. The peels of pomegranate (*Punica granatum* L.) were collected from a juice factory on 6 October, in Giza City, Egypt.

2.2 Preparation of PPE

The outside and inner portions of pomegranate peels were firstly cleaned with tap water, and dried at 80 °C for about 24 h. After the drying process, the peels were crushed in a mixer and finally sieved by a 20-mesh sieve screen. About 10 g of the obtained fine peel powder was dissolved in 100 ml distilled water and heated for about half an hour at 85 °C. Finally, the filter paper used for vacuum filtration is Whatman No. 1 filter paper which is applied for getting the final filtered liquid extract as mentioned in the following reference with some modifications [32]. The definitive part of the extract was adapted to 100 ml with sterilized distilled water and maintained in an amber bottle (at 4 °C) for additional investigations.

2.3 Biosynthesis of bimetallic Ag-ZnO NPs using PPE

For the purpose of bimetallic biosynthesis, the distinct amount of salts was used for Ag-ZnO NPs biosynthesis. In details, 10 ml of (2.0 mM) Zn $(NO_3)_2 \cdot 6H_2O$ was mixed with 10 ml (2.0 mM) $AgNO_3$ and stirring at room temperature for about 30 min. Then they were mixed with 80 ml of the created PPE. After preparing the mixture solution, we check the solution pH and it was found to be 7.2. The reaction parameters were prepared as the incubation temperature set at 30 °C, and reaction time of about 24 h under agitation (250 rpm) in a shaking incubator, which were adapted to develop the most profitable synthesis of bimetallic Ag-ZnO NPs [33]. After the complete incubation, we noted the change in color and fixed it as faint brown which demonstrated the bimetallic Ag-ZnO NPs bio-formation. Finally, the synthesized bimetallic Ag-ZnO NPs were clarified by centrifugation at 7500 rpm for about 15 min and must be cleaned five times with distilled water to draw loosely bound peel biomolecules.

2.4 Ag-ZnO NPs validation

Firstly, the optical property of the formed bimetallic Ag-ZnO NPs was tested by UV-Vis. spectrophotometer (JASCO V-560) at distinct wavelengths in the range from 190 to 900 nm. It must be mentioned that we must auto-zero the instrument by the sample without the known metal salt before the measurements. For the average particle size diffusion of the produced bimetallic Ag-ZnO NPs, we conduct dynamic light scattering (DLS-PSS-NICOMP 380, USA).

Additionally, the average and exact size of the formed bimetallic Ag-ZnO NPs and the noted shapes of the synthesized Ag-ZnO NPs were determined by HR-TEM (HR-TEM, JEM2100, Jeol, Japan). The crystallinity and the crystal size determination were investigated after conducting XRD (XRD-6000, Shimadzu Scientific Instruments, Japan). The surface morphology and boundary size of the synthesized bimetallic Ag-ZnO NPs were assessed by SEM (SEM, ZEISS, EVO-MA10, Germany). In addition, the elemental arrangement, purity, and dispersal of components established in the synthesized Ag-ZnO NPs were determined by EDX, BRUKER, Germany.

Additionally, FTIR analysis (JASCO FT-IR 3600, KBr Pellet method, and wavenumber range from 400 to 4000 cm^{-1}) was carried out to reveal chemical functional groups established between the prepared bimetallic Ag-ZnO NPs and PPE.

2.5 Antibacterial activity

Antibacterial activity of bimetllic Ag-ZnO NPs, zinc nitrate, silver nitrate, and PPE was evaluated against Gram-negative (*Pseudomonas aeruginosa* ATCC 27853, *Escherichia coli* ATCC 25922) and Gram-positive bacteria (*Bacillus subtilis* ATCC 6051, *Enterococcus faecalis* ATCC 29212, *Staphylococcus aureus* ATCC 25923) using agar well diffusion method according to document M51-A2 of CLSI [34] with minor modifications. Bacterial suspensions of 1.5×10^7 CFU/ml were separately prepared, seeded into Muller Hinton agar media, and poured under septic conditions into sterilized Petri plates. In each plate, four agar wells (7 mm) were made using a cork-porer, and then 100 µl of bimetallic Ag-ZnO NPs, zinc nitrate, silver nitrate, and PPE at a concentration of 1000 µg/ml was transferred to wells separately. Then plates were put in the refrigerator for 2 h followed by incubation at 37 °C for 24 h. and then the inhibition zone diameter was measured. Different concentrations of Ag-ZnO NPs and PPE ranging from 1000 to 3.9 µg/mL were used to detect MIC [35].

2.6 Antifungal activity

Also, antifungal activity was assessed toward *Candida albicans* ATCC 90028, *Cryptococcus neoformans* ATCC 14116, *Aspergillus fumigatus* ATCC 204305, and *A. brasiliensis* ATCC 16404 using the agar well diffusion method. Fungal suspensions were uniformly distributed on agar potato dextrose agar (PDA) plates individually. Then, 100 µl of each bimetallic Ag-ZnO NPs, zinc nitrate, silver nitrate, and PPE at a concentration of 1000 µg/ml was added and was put in agar wells (7 mm) separately. All plates were incubated at 30 °C for 3 days, and then inhibition zones were measured. Different concentrations of Ag-ZnO NPs and PPE ranging from 1000 to 3.9 µg/ml were tested as an antifungal to detect MIC [35].

2.7 Cytotoxicity and anticancer activity

MTT (3-(4,5-dimethylthiazol-2-yl)-2,5-diphenyl-2H-tetrazolium bromide) (Bio Basic Inc. Canada) assay protocol was used to check the cytotoxicity of the prepared bimetallic Ag-ZnO NPs [36]. The normal Vero cell line and cancerous cell lines MCF7 (breast cancer) and Caco2 (colorectal adenocarcinoma) were collected from American Type Culture Collection (ATCC). The viability and inhibition percentages were calculated according to these equations:

$$\text{Viability } \% = \frac{\text{Sample optical density}}{\text{Control opticald ensity}} \times 100$$

$$\text{Inhibition } \% = 100 - \text{Viability } \%$$

3 Results and discussion

3.1 Bimetallic Ag-ZnO NP biosynthesis using PPE

Fruit peel wastes are a valuable source of phytochemicals which have an essential role in nanocomposite production. Different plant organ extracts showed different results during nanoparticle production [37]. The production of bimetallic Ag-ZnO NPs by PPE was observed in this study by a change in solution color to faint brown color, which operated as a reducing agent or capping agent to reduce zinc nitrate and silver nitrate into bimetallic Ag-ZnO NPs and stabilize them in a colloidal form. The bioactive phytochemicals from plant extracts serve as a capping agent, preventing nanoparticle aggregation and altering their biological activity [38, 39]. Yilmaz et al. [40] indicated that the watermelon and pomegranate peel extracts have a higher total phenolic content which helps in the reduction of silver ions to Ag NPs.

The main phytochemicals present in plant peels are flavones, terpenoids, sugars, ketones, aldehydes, carboxylic acids, and amides, which are responsible for the bioreduction and NPs synthesis [41]. Flavonoids contain various functional groups, which have an enhanced ability to reduce metal ions. The reactive hydrogen atom is released due to tautomeric transformations in flavonoids by which enol-form is converted into the keto-form. This process is realized by the reduction of metal ions into metal NPs [42].

3.2 Characterization of the biosynthesized bimetallic Ag-ZnO NPs

PPE filtrate was tested for its capability regarding bimetallic Ag-ZnO NPs biosynthesis. The color of the PPE seemed brown, which shifted to faint brown concerning the biosynthesis of bimetallic Ag-ZnO NPs. The produced pale brown color was assigned to the stimulation of biogenic Ag-ZnO NPs' surface plasmon resonance and provided a correct spectroscopic signal of their appearance [43].

The UUV Vis. spectra exhibited the experimental peak (Fig. 1) conducting the O. D. (1.029; diluted 5 times), and the bimetallic Ag-ZnO NPs were diminutive in size, which was observed at 395.0 nm, according to the UV-Vis. analyses. The existence of filtrate peaks is shown by the UV-Vis. spectrum of the produced PPE, which matches the literature studies [44, 45]. The intensity of the brown constructed was fitting to the power of the prepared PPE to biosynthesize Ag-ZnO NPs [25, 46]. Additionally, the detected peaks from 250 to 300 nm in the Ag-ZnO NP spectrum corresponded to the

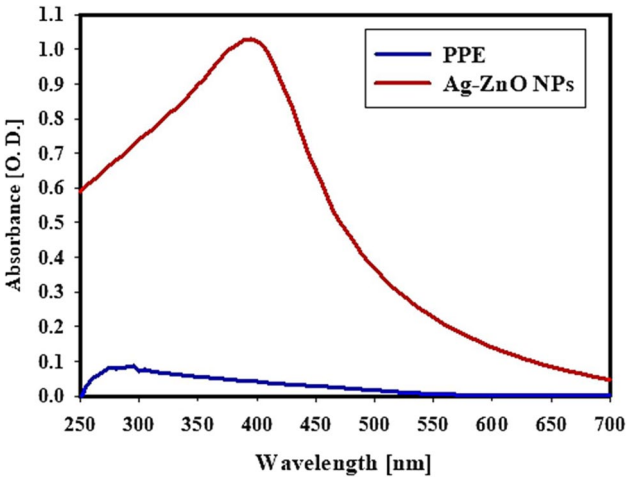

Fig. 1 UV-Vis. spectra of the synthesized bimetallic Ag-ZnO NPs, and the prepared PPE

PPE constituents. Usually, surface plasmon resonance (SPR) is influenced by the intensity, dimension, morphological surfaces, and structure and dielectric manners of any constructed nanoparticles [47, 48].

To investigate the average size of the biosynthesized bimetallic Ag-ZnO NPs, HR-TEM analysis was performed, and its outcomes were likened to the DLS investigation, which operated to define the hydrodynamic radius, particle size distribution, and polydispersity index (PDI) [49]. HR-TEM image represented the spheroidal forms with moderately mono-dispersed Ag-ZnO NPs with a common size from 9.5 to 25.2 nm. The mean diameter was calculated to be 15.8 ± 1.5 nm, as shown in Fig. 2a. The delivered mono-dispersed bimetallic Ag-ZnO NPs were appointed to the prepared PPE rich in protein and amino acid, etc. This was supposed to reduce, stabilize, and cap agents [50]. In HRTM imaging (Fig. 2a), the line spacing was the same indicating one phase structure. It can be suggested that silver was homogeneously distributed within the zinc oxide matrix forming an alloy. The radical-multi-position of PPE may cause simultaneous reduction of both Ag and Zn as mentioned in the published article [51].

By making a comparison in the literature regarding the average particle size and shape, it was found that our synthesized bimetallic Ag-ZnO NPs were small in size, and a major shape is spherical. Castro-Longoria et al. [52] synthesized silver, gold, and silver-gold bimetallic NPs by a green method utilizing the extract of a filamentous fungus, and the shape of NPs was found to be mainly spherical with an average diameter of 11.0 nm for silver and 32.0 nm for gold, when the fungus was exposed to the aqueous solutions of 10^{-3} M of $AgNO_3$ and $HAuCl_4$, respectively.

The produced shapes may be varied in that study [52], since the shape of extracted NPs was nearly spherical or

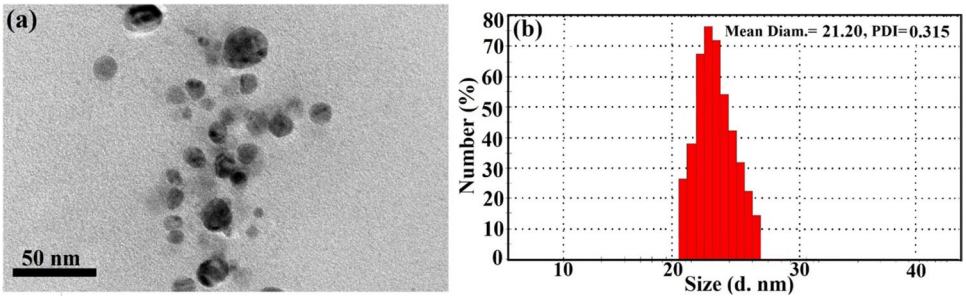

Fig. 2 Mean particle size, shape, particle size distribution and PDI determination of the synthesized bimetallic Ag-ZnO NPs, where **a** HRTEM imaging, and **b** DLS analysis

ellipsoidal in all cases, although other morphologies may be observed due to the synthetic process from extract so the anisotropic shape had been noted. In our study, a fixed shape is displayed due to the single reducing and capping agents being applied (PPE).

The DLS technique defined the typical particle size distribution and was estimated as 21.20 nm in the bimetallic Ag-ZnO NPs biosynthesized by the prepared PPE (Fig. 2b).

International standard organizations (ISOs) have demonstrated that polydispersity index (PDI) values less than 0.05 are more expected to monodisperse models. In contrast, values more than 0.7 are expected to be a polydispersity diffusion of particles [53]. Herein, for the accepted PDI values (Fig. 2b), the PDI value was 0.315. The current values demonstrate that the biosynthesized bimetallic Ag-ZnO NPs were a moderate mono-size spread.

From the obtained results, the mean and predominate size calculated from DLS analysis was greater than the size of the particles estimated from the HRTEM imaging. The causes are defined as the DLS method considered the hydrodynamic radius within the biosynthesized Ag-ZnO NPs and surrounded via the water layers concerning the considerable sizes of the biosynthesized bimetallic Ag-ZnO NPs as described in the following reference [54].

The surface features and surface shape of the produced bimetallic Ag-ZnO NPs were investigated via SEM technique. The date in Fig. 3a depicts the SEM analysis of the PPE, which seems as irregular flakes aggregated as bulk organic materials. On the other hand, SEM images of bimetallic Ag-ZnO NPs biosynthesized by the prepared PPE with variable boundary size and the equivalent spherical particles were located within the PPE (Fig. 3b). Moreover, the SEM results of bimetallic Ag-ZnO NPs (Fig. 3b), combined with PPE, exhibit uniform Ag-ZnO NPs surfaces, and the surface appearance was clear. It can be detected that bimetallic Ag-ZnO NPs were isolated typically as a rounded particle across the PPE, which shows as brilliant NPs combined and stabilized with the prepared PPE. By making a comparison in the literature regarding the morphological shape and elemental analysis, it was found that the synthesized bimetallic Ag-ZnO NPs (in this study) were uniformly distributed with narrow size and the same spherical shape. Muhammad Mohsin et al. [55] synthesized bimetallic silver and gold core-shell NPs by citrate reduction method at different temperatures and pH. The obtained morphological shape and boundary size indicated that they have possessed a size ranging from 50 to 65 nm and appear as spherical particles, so the temperature and pH play a vital part in the production process.

The EDX examination is a rational approach used for the fundamental analysis or the chemical characterization of the synthesized specimens [56]. EDX analysis was employed to demonstrate the primary form, and true structure of the biosynthesized bimetallic Ag-ZnO NPs and the purity (Fig. 3d). Ag NPs revealed specific absorption peaks of Ag element at 2.71 keV; additionally, ZnO NPs exhibited specific absorption peaks of zinc element at 1.12 keV and oxygen at 0.51 keV. The relative elemental percentage for Ag was 12.5%, Zn was 19.4%, and O was 10.4%, while C for the remaining PPE possessed an elemental percentage of 57.7%. EDX examination of the prepared PPE (Fig. 3c) represented the essential peaks that correspond to the basic atoms found in the filtrate (O, C, Na, K, and Cl).

XRD studies for bimetallic Ag-ZnO NPs are illustrated in Fig. 4a. XRD results regarding the produced bimetallic Ag-ZnO NPs represent the amorphous, and crystal arrangements for the precursor (PPE) and the biosynthesized bimetallic Ag-ZnO NPs. It must be noted that 2θ at 22.21° (donated as *) corresponds to the amorphous PPE (amino acids and total phenolic content) [19, 57]. XRD results of the biosynthesized bimetallic Ag-ZnO NPs in Fig. 4a illustrated the XRD diffraction peaks of Ag NPs including peaks at 2θ = 38.49°, 44.09°, 63.90°, and 78.31° which corresponded with a traditional card JCPDS-ICDD number 04-0783, and resembled to (111), (200), (220), and (311) Bragg's reflections [58].

Also, Fig. 4a displays the XRD diffraction peaks of ZnO NPs including peaks at 2θ = 27.50°, 47.15°, 56.80°, 66.58°, and 71.25° which complemented with a typical card JCPDS number 361451, and corresponding to (002), (101), (102), (110), (103), and (201) Bragg's reflections [59], indicating that the produced bimetallic Ag-ZnO NPs were crystal in character and delivered the face-centered cubic (fcc) crystalline design. Ultimately, there is exclusively one undeveloped peak at

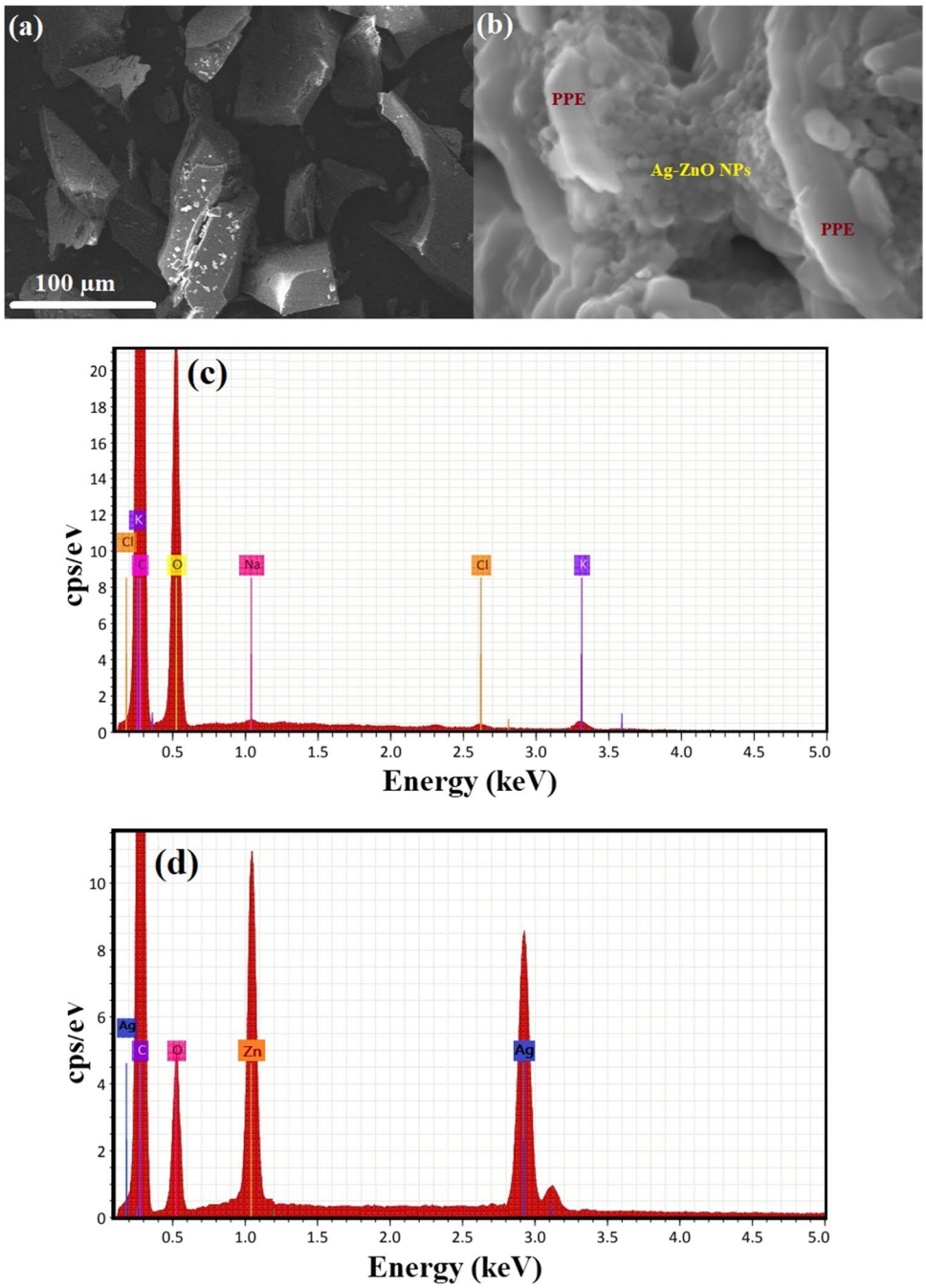

Fig. 3 Morphological surface determination, and elemental analysis where **a** SEM imaging of the prepared PPE, **b** SEM imaging of the biosynthesized bimetallic Ag-ZnO NPs, **c** EDX spectrum of the prepared PPE, and **d** EDX spectrum of the biosynthesized bimetallic Ag-ZnO NPs

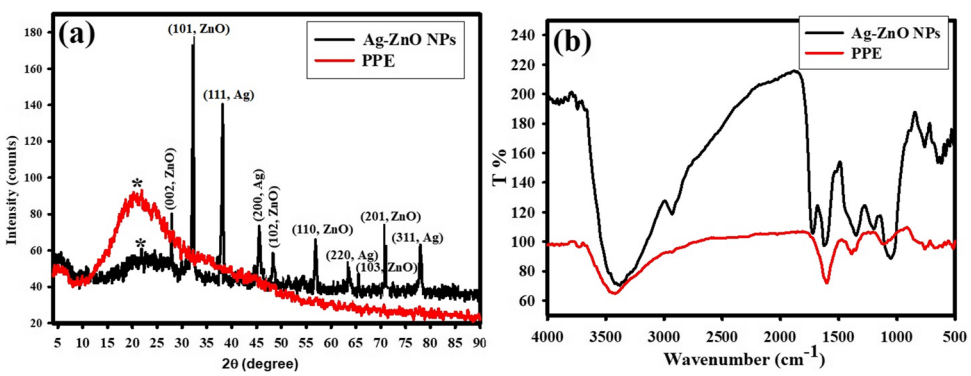

Fig. 4 Crystallinity, surface bonding and functional groups analysis of PPE and the biosynthesized bimetallic Ag-ZnO NPs where **a** XRD spectra of the prepared PPE, and bimetallic Ag-ZnO NPs, and **b** FTIR spectra of the prepared PPE, and bimetallic Ag-ZnO NPs

23.50° (donated as *) regarding PPE validation (Fig. 4a) which is interested in the synthesis and strength of bimetallic Ag-ZnO NPs. Nevertheless, its intensity was more straightforward than that noticed in PPE, and 2θ was shifted because of the incorporation of bimetallic Ag-ZnO NPs into the active PPE. The XRD results indicate that the produced bimetallic Ag-ZnO NPs were highly crystalline and conjugated with amorphous PPE which increased its distribution in the solution for better biomedical application [60].

Finally, the mean bimetallic Ag-ZnO NP crystallite size was defined by the equation of Williamson-Hall (W H) [61, 62] and was observed to be 13.85 nm according to Eq. 1.

$$\beta \cos \theta = \frac{k\lambda}{D_{W-H}} + 4\varepsilon \sin \theta \quad (1)$$

Figure 4b displayed the FTIR range of PPE and the biosynthesized bimetallic Ag-ZnO NPs. The FTIR spectrum of PPE demonstrated the complicated character of the peels and confirmed the existence of a broad assortment of combinations. Investigations have noted that pomegranate peels possess additional biological mixtures with natural character [63–65].

From Fig. 4b, it marked that the PPE spectrum revealed vast bandwidth of 3419 cm^{-1} and demonstrates the O–H stretching band ensures the existence of alcohol and carboxylic acids. The C=C stretching band of the alkyne group was seen at band 2923 cm^{-1}. The blunt mid-intense peak at 1728 cm^{-1} was due to carbonyl group C = O indicating the presence of ketones, aldehydes, and carboxylic acids. The short moderate peak at 1605 cm^{-1} shows the existence of unsaturated combinations (alkenes), and the bands located at 1389 cm^{-1} for –O-CH_3 deformation. The band at 1343 cm^{-1} (CH_2 bending) is connected to cellulose's existence; a peak at 1115 cm^{-1} (-CH_3CO stretching) demonstrates the existence of ethers and esters.

Finally, a noted peak at 769 cm^{-1} for -CCH and –COH bending, from Fig. 4b, can attend that the PPE spectrum are identical to that declared in the literature review [65, 66].

Finally, the FTIR spectrum of bimetallic Ag-ZnO NPs biosynthesized by PEE indicated the same peaks detected in the FTIR spectrum of PPE alone, but a separate peak at 632 cm^{-1} was seen within FTIR of bimetallic Ag-ZnO NPs only, which may be because of the connection and a cross of Ag or Zn NPs within the hydroxyl group as Ag–O or Zn–O.

The FTIR results determined that the strength of peaks was slightly changed within the bimetallic Ag-ZnO NPs spectrum, which may be due to the physical incorporation of bimetallic Ag-ZnO NPs across the hydroxyl group (intermolecular hydrogen bonding [67, 68]) and the other functional groups presented in PEE. The absence of additional non-identified peaks suggested the purity of the synthesized sample and all the peaks were in the same wavenumbers indicating the similarity in the incorporation and/or conjugation of the synthesized bimetallic Ag-ZnO NPs throughout the main functional groups of the stabilizer PPE [69].

3.3 Biological studies

3.3.1 Antibacterial activity

The antibacterial activity of starting materials (PPE, silver nitrate, and zinc nitrate) and bimetallic Ag-ZnO NPs toward Gram-positive and Gram-negative bacteria were assessed (Fig. 5). Results revealed that bimetallic Ag-ZnO NPs at a concentration of 1000 µg/ml exhibited potential antibacterial activity toward *P. aeruginosa*, *E. coli*, *B. subtilis*, *S. aureus*, and *E. faecalis* where inhibition zones were 24.2, 17.6, 32.1, 21.7, and 14.9 mm respectively. Moreover, *B. subtilis* was the most sensitive toward bimetallic Ag-ZnO NPs where MIC was 15.62 µg/ml, while *E. faecalis* was the least sensitive where MIC was 250 µg/ml. Also, MICs of bimetallic Ag-ZnO NPs against *E. coli*, *P. aeruginosa*, and *S. aureus* were 62.5, 125, and 62.5 µg/ml, respectively.

On the other hand, PPE exhibited weak antibacterial activity against *E. coli* and *B. subtilis* only. Also, both silver nitrate and zinc nitrate did not exhibit any activity on all tested bacterial strains. This indicates that the efficacy of bimetallic Ag-ZnO NPs is not attributed to their starting material but attributed to the effect of the prepared nanoparticles (bimetallic Ag-ZnO NPs). Ibănescu et al. [70] reported that Ag-ZnO NPs had antibacterial activity against *E. coli* and *Micrococcus luteus*. Also, Ag-ZnO NPs exhibited antibacterial activity against *P. aeruginosa* and *S. aureus* [71–73]. The mechanism of action of bimetallic Ag-ZnO NPs may be attributed to electrostatic interaction which causes cell membrane damage, disruption of proteins and enzymes, ROS generation and oxidative stress, protein binding which leads to homeostasis disturbance (electron transport chain disruption), signal transduction inhibition, and genotoxicity [74, 75]. Also, the efficacy may be attributed to the roughness of the external surface of Ag-ZnO NPs which causes damaging the cell wall; these lead to penetrating Ag-ZnO NPs to the plasma membrane and causing toxicity to bacteria as reported by Zhang, Jiang, Ding, Povey and York [76].

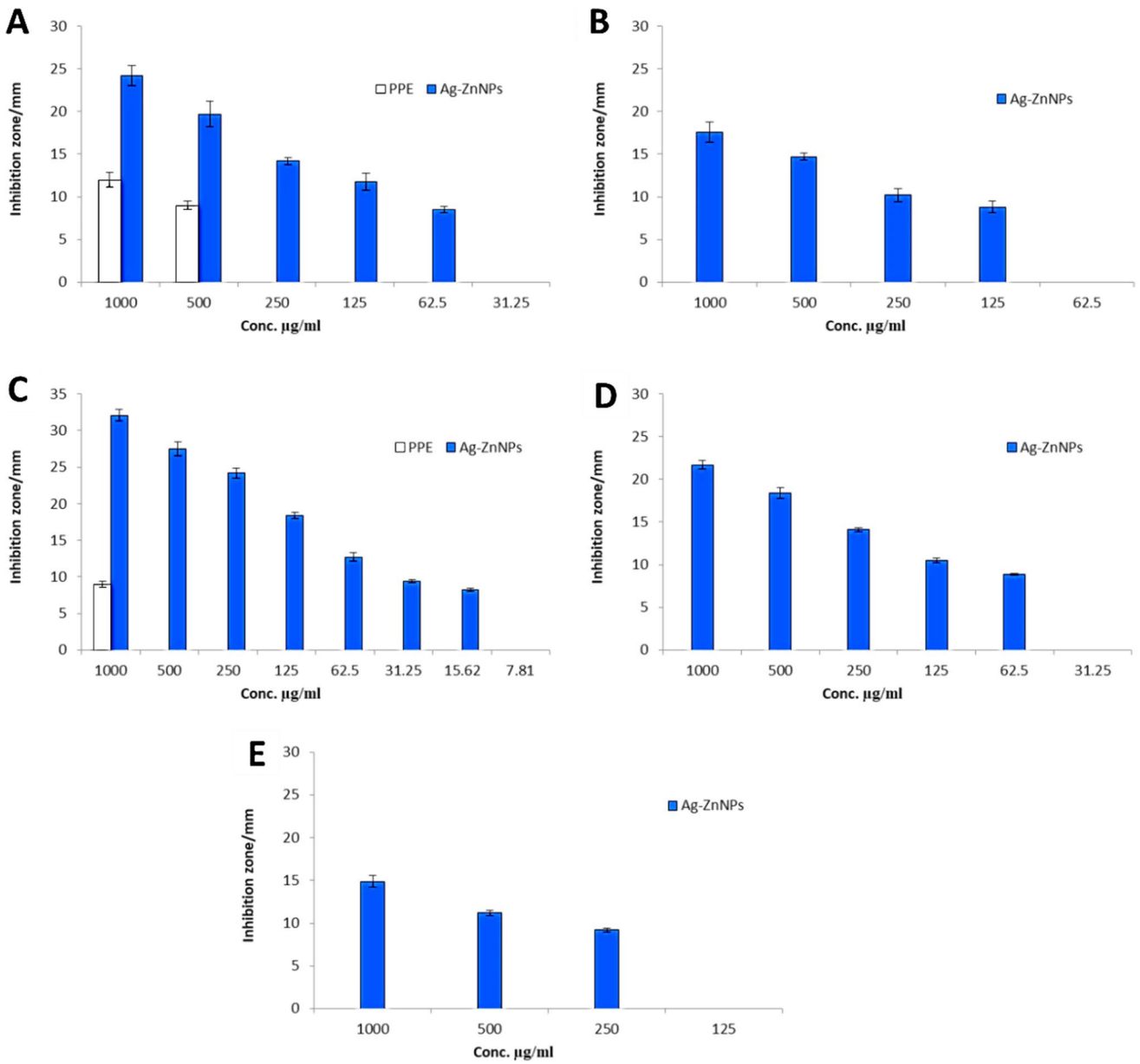

Fig. 5 Antibacterial activity of bimetallic Ag-ZnONPs and PPE against *E. coli* (**A**), *P. aeruginosa* (**B**), *B. subtilis* (**C**), *S. aureus* (**D**) and *E. faecalis* (**E**)

3.3.2 Antifungal activity

Antifungal activity of the starting materials and bimetallic Ag-ZnO NPs toward *C. albicans*, *C. neoformans*, *A. brasiliensis*, and *A. fumigatus* was shown in (Fig. 6). Results illustrated that bimetallic Ag-ZnO NPs have antifungal efficacy toward unicellular as well as multicellular fungi. The prepared bimetallic Ag-ZnO NPs exhibited antifungal activity against *C. albicans*, *C. neoformans*, *A. brasiliensis*, and *A. fumigatus*, where inhibition zones at a concentration of 1000 µg/ml were 38.3, 34.8, 31.4, and 21.7 mm, respectively.

Additionally, MIC of bimetallic Ag-ZnO NPs toward each tested fungal strain was detected as shown in Fig. 6. Results of MIC showed that MICs of bimetallic Ag-ZnO NPs against *C. albicans*, *C. neoformans*, *A. brasiliensis*, and *A. fumigatus* were 7.81, 31.25, 62.5, and 125 µg/ml, respectively. These confirms that bimetallic Ag-ZnO NPs have high efficacy toward unicellular more than multicellular fungi. Moreover, *C. albicans* were the most sensitive strains among other tested strains.

On the other hand, silver nitrate and zinc nitrate did not give any activity, while PPE exhibited weak antifungal activity at higher concentrations (500–1000 µg/ml). Previous studies

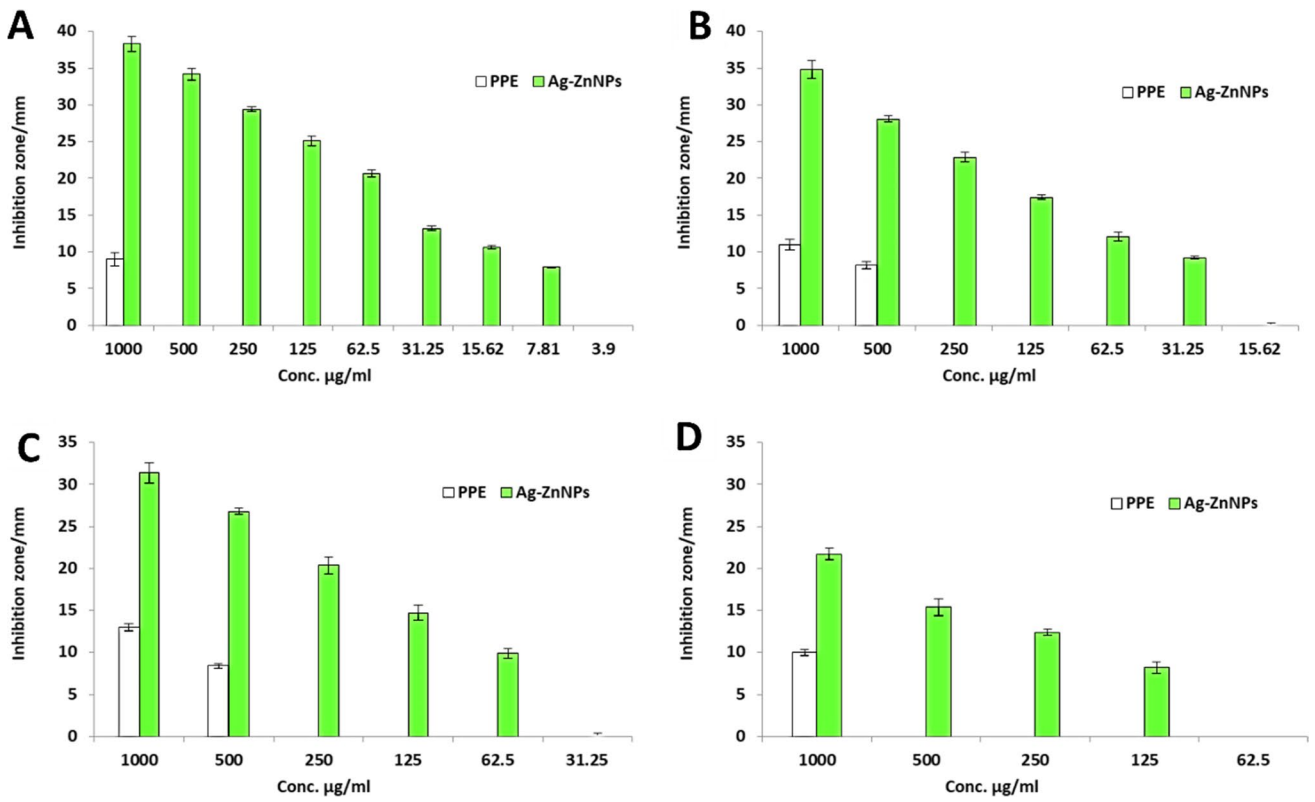

Fig. 6 Antifungal activity of bimetallic Ag-ZnONPs and PPE against *C. albicans* (**A**), *C. neoformans* (**B**), *A. brasiliensis* (**C**), *A. fumigatus* (**D**)

confirmed the antifungal activity of bimetallic nanoparticles [73, 77]. A previous study reported that Ag-ZnO NPs showed potential antifungal activity toward *C. albicans* [73]. Likewise, Zaheer and Albukhari [73] reported that ZnO-AgNPs have promising antifungal activity against *C. albicans*. Gutiérrez et al. [78] synthesized bimetallic Au–Ag NPs and found that these nanoparticles have antifungal activity against *C. parapsilosis*, *C. Krusei*, *C. glabrata*, *C. guillermondii*, and *C. albicans.*

3.4 Cytotoxicity anticancer activity

To check the biosafety of the prepared bimetallic compounds, cytotoxicity against normal cell lines is required. Therefore, the cytotoxicity of bimetallic Ag-ZnO NPs toward Vero cells was evaluated as shown in Fig. 7B. Cytotoxicity of different concentrations of bimetallic Ag-ZnO NPs (1000 to 31.25 µg/ml) was evaluated. Results illustrated that the IC_{50} of bimetallic Ag-ZnO NPs was 155.1 µg/ml. Thus, the prepared bimetallic Ag-ZnO NPs in the current study are safe to use because if IC_{50} is greater than 90 µg/ml, the material is classified as non-cytotoxic [79].

Anticancer activity of biosynthesized bimetallicA g-ZnO NPs was carried out against MCF7 and Caco2 as cancerous cell lines (Fig. 7A and B). Results revealed that bimetallic Ag-ZnO NPs exhibited anticancer activity against both MCF7 and Caco2 cancerous cell lines where IC_{50} was 104.9 and 52.4 µg/ml, respectively. Moreover, the anticancer activity of bimetallic Ag-ZnO NPs toward MCF7 at concentrations 1000, 500, 250, and 125 µg/mL were 97.7, 97.6, 93.2, and 67.1%, respectively.

Likewise, bimetallic Ag-ZnO NPs exhibited promising anticancer activity against Caco2, which were 96.2, 95.1, 92.3, 89.2, and 70.87% at concentrations 1000, 500, 250, 125, and 62.5 µg/ml, respectively. Ambujakshi et al. [80] reported that biosynthesized Ag-ZnO NPs using *Chonemorpha grandiflora* leaf extract was tested towards MCF 7, HCT 116, and A 549 cell lines.

Elsayed et al. [81] fabricated ZnO-Ag NPs using laser ablation and found that these particles have anticancer activity against HCT 116 and HeLa cancerous cell lines. Finally, Pandiyan et al. [82] reported that the nanocomposite (Ag-Au/ZnO) has potential anticancer activity toward human cervical cancerous cells (HeLa).

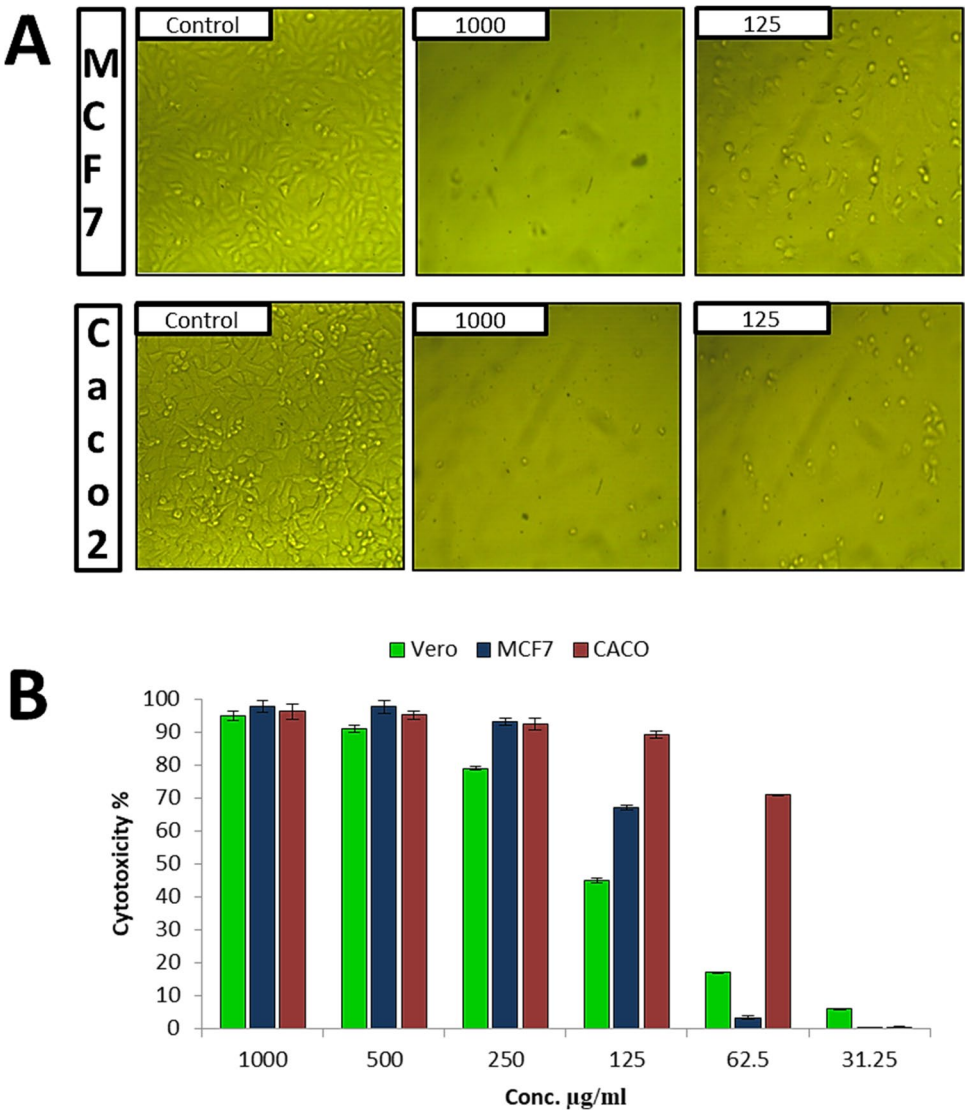

Fig. 7 Cytotoxicity of Vero, MCF7 and Caco2 A-B: **A** inhibition of cells, **B** cytotoxicity %

4 Conclusion

In the current study, the novelty and scientific significance concentrated on the biogenic synthesis of bimetallic Ag-ZnO NPs using PPE for the first time, for increasing the synergistic activity at a low concentration (to avoid toxicity) and elevate the superior potential. The UV-Vis. spectra exhibited a noted peak at the O. D. (1.029; diluted 5 times), and the bimetallic Ag-ZnO NPs were small in size (15.8 nm), which was observed at 395.0 nm. The SEM image of the PPE looks like irregular flakes aggregated as bulk organic materials; also, the SEM image of bimetallic Ag-ZnO NPs has a variable boundary size, and the equivalent spherical particles were located within the PPE. The FTIR results determined that the strength of peaks was slightly changed within the bimetallic Ag-ZnO NP spectrum, which may be due to the physical incorporation of bimetallic Ag-ZnO NPs across the hydroxyl group by intermolecular hydrogen bonding. The biosynthesized bimetallic Ag-ZnO NPs at a concentration of 1000 µg/ml exhibited potential antibacterial activity toward *P. aeruginosa*, *E. coli*, *B. subtilis*, *S. aureus*, and *E. faecalis* where inhibition zones were 24.2, 17.6, 32.1, 21.7, and 14.9 mm, respectively. The prepared bimetallic Ag-ZnO NPs (1000 µg/ml) exhibited antifungal activity against *C. albicans*, *C. neoformans*, *A. brasiliensis*, and *A. fumigatus* where inhibition zones were 38.3, 34.8, 31.4, and 21.7 mm, respectively. Results revealed that bimetallic Ag-ZnO NPs exhibited anticancer activity against both MCF7 and Caco2 cancerous cell lines, where IC_{50} was 104.9 and 52.4 µg/mL, respectively. According to the promising results, the prepared eco-friendly and cost-effective bimetallic Ag-ZnO NPs may be used in the biomedical fields as smart and encouraging agents.

Author contribution AHH suggested the research topic, investigated the article, planned the research methodology, wrote the original draft, and participated in data representation and article revising and editing.

GSE suggested the research topic, investigated the article, planned the research methodology, wrote the original draft, and participated in data representation and article revising and editing.

Funding Open access funding provided by The Science, Technology & Innovation Funding Authority (STDF) in cooperation with The Egyptian Knowledge Bank (EKB).

Data availability The datasets used and analyzed during the current study are available from the corresponding author on reasonable request.

Declarations

Ethical approval Not applicable.

Consent to participate Not applicable.

Conflict of interest The authors declare no competing interests.

Research involving human participants and/or animals Not applicable.

References

1. Hawash M, Jaradat N, Eid AM, Abubaker A, Mufleh O, Al-Hroub Q, Sobuh S (2022) Synthesis of novel isoxazole–carboxamide derivatives as promising agents for melanoma and targeted nano-emulgel conjugate for improved cellular permeability. BMC Chem 16(1):47
2. Chang Y-L, Yu S-J, Heitman J, Wellington M, Chen Y-L (2017) New facets of antifungal therapy. Virulence 8(2):222–236
3. Campoy S, Adrio JL (2017) Antifungals. Biochem Pharmacol 133:86–96
4. Schwartsmann G (2001) Breast cancer in South America: challenges to improve early detection and medical management of a public health problem. J Clin Oncol 19(18 Suppl):118S-124S
5. Rabiee N, Bagherzadeh M, Kiani M, Ghadiri AM, Etessamifar F, Jaberizadeh AH, Shakeri A (2020) Biosynthesis of copper oxide nanoparticles with potential biomedical applications. Int J Nanomed 15:3983
6. Abdelaziz AM, Salem SS, Khalil AMA, El-Wakil DA, Fouda HM, Hashem AH (2022) Potential of biosynthesized zinc oxide nanoparticles to control Fusarium wilt disease in eggplant (Solanum melongena) and promote plant growth. Biometals 35(3):601–616
7. Hashem AH, Al Abboud MA, Alawlaqi MM, Abdelghany TM, Hasanin M (2022) Synthesis of nanocapsules based on biosynthesized nickel nanoparticles and potato starch: antimicrobial, antioxidant, and anticancer activity. Starch-Stärke 74(1–2):2100165
8. El-Naggar ME, Hasanin M, Hashem AH (2022) Eco-friendly synthesis of superhydrophobic antimicrobial film based on cellulose acetate/polycaprolactone loaded with the green biosynthesized copper nanoparticles for food packaging application. J Polym Environ 30(5):1820–1832
9. Saied E, Hashem AH, Ali OM, Selim S, Almuhayawi MS, Elbahnasawy MA (2022) Photocatalytic and Antimicrobial activities of biosynthesized silver nanoparticles using Cytobacillus firmus. Life 12(9):1331
10. Hashem AH, Saied E, Amin BH, Alotibi FO, Al-Askar AA, Arishi AA, Elkady FM, Elbahnasawy MA (2022) Antifungal activity of biosynthesized silver nanoparticles (AgNPs) against Aspergilli causing aspergillosis: ultrastructure study. J Funct Biomater 13(4):242
11. Zhang X, Yan S, Tyagi R, Surampalli R (2011) Synthesis of nanoparticles by microorganisms and their application in enhancing microbiological reaction rates. Chemosphere 82(4):489–494
12. Shah M, Fawcett D, Sharma S, Tripathy SK, Poinern GEJ (2015) Green Synthesis of metallic nanoparticles via biological entities. Materials (Basel, Switzerland) 8(11):7278–7308
13. Sharma D, Kanchi S, Bisetty K (2019) Biogenic synthesis of nanoparticles: a review. Arab J Chem 12(8):3576–3600
14. Hasanin M, Hashem AH, Lashin I, Hassan SAM (2021) In vitro improvement and rooting of banana plantlets using antifungal nanocomposite based on myco-synthesized copper oxide nanoparticles and starch. Biomass Conv Bioref (in press). https://doi.org/10.1007/s13399-021-01784-4
15. Hashem AH, Selim TA, Alruhaili MH, Selim S, Alkhalifah DHM, Al Jaouni SK, Salem SS (2022) Unveiling antimicrobial and insecticidal activities of biosynthesized selenium nanoparticles using prickly pear peel waste. J Funct Biomater 13(3):112
16. Ali OM, Hasanin MS, Suleiman WB, Helal EE-H, Hashem AH (2022) Green biosynthesis of titanium dioxide quantum dots using watermelon peel waste: antimicrobial, antioxidant, and anticancer activities. Biomass Conv Bioref (in press). https://doi.org/10.1007/s13399-022-02772-y
17. Saied E, Salem SS, Al-Askar AA, Elkady FM, Arishi AA, Hashem AH (2022) Mycosynthesis of Hematite (α-Fe2O3) Nanoparticles using Aspergillus niger and their antimicrobial and photocatalytic activities. Bioengineering 9(8):397
18. Albalawi MA, Abdelaziz AM, Attia MS, Saied E, Elganzory HH, Hashem AH (2022) Mycosynthesis of silica nanoparticles using aspergillus niger: control of Alternaria solani causing early blight disease, induction of innate immunity and reducing of oxidative stress in eggplant. Antioxidants 11(12):2323
19. Hashem AH, Saied E, Ali OM, Selim S, Al Jaouni SK, Elkady FM, El-Sayyad GS (2023) Pomegranate peel extract stabilized selenium nanoparticles synthesis: promising antimicrobial potential, antioxidant activity, biocompatibility, and hemocompatibility. Appl Biochem Biotechnol (in press). https://doi.org/10.1007/s12010-023-04326-y
20. Salem SS, Ali OM, Reyad AM, Abd-Elsalam KA, Hashem AH (2022) Pseudomonas indica-mediated silver nanoparticles: antifungal and antioxidant biogenic tool for suppressing mucormycosis fungi. J Fungi 8(2):126
21. Radhakrishnan Arya P, Abishad P, Unni V, Vemula Ram P, Pollumahanti N, Yasur J, John L, Karthikeyan A, Nambiar P, Juliet S, Kunjukunju Vinod V, Vergis J, Vasantrao Kurkure N, Baliram Barbuddhe S, Byrappa K, Bhiwa Rawool D (2023) Facile synthesis of silver-zinc oxide nanocomposites using Curcuma longa extract and its in vitro antimicrobial efficacy against multi-drug

resistant pathogens of public health importance. Inorg Chem Commun 148:110356
22. Panwar A, Yadav KL (2022) Silver doped zinc oxide nanostructures with antibacterial properties against GFP-expressing antibiotic resistant Escherichia coli. Mater Lett 309:131469
23. Abdel Maksoud M, Awed A, Sokary R, Bekhit M (2021) Effect of gamma irradiation on the free-standing polyvinyl alcohol/chitosan/Ag nanocomposite films: insights on the structure, optical, and dispersion properties. Appl Phys A 127(8):1–11
24. Sohrabnezhad S, Seifi A (2016) The green synthesis of Ag/ZnO in montmorillonite with enhanced photocatalytic activity. Appl Surf Sci 386:33–40
25. Khatami M, Varma RS, Zafarnia N, Yaghoobi H, Sarani M, Kumar VG (2018) Applications of green synthesized Ag, ZnO and Ag/ZnO nanoparticles for making clinical antimicrobial wound-healing bandages. Sustain Chem Pharm 10:9–15
26. Alharthi FA, Alghamdi AA, Al-Zaqri N, Alanazi HS, Alsyahi AA, Marghany AE, Ahmad N (2020) Facile one-pot green synthesis of Ag–ZnO nanocomposites using potato peeland their Ag concentration dependent photocatalytic properties. Sci Rep 10(1):20229
27. Noohpisheh Z, Amiri H, Farhadi S, Mohammadi-gholami A (2020) Green synthesis of Ag-ZnO nanocomposites using Trigonella foenum-graecum leaf extract and their antibacterial, antifungal, antioxidant and photocatalytic properties. Spectrochim Acta Part A Mol Biomol Spectrosc 240:118595
28. Nguyen TM-T, Nguyen TA-T, Tuong-Van Pham N, Ly Q-V, Tran TT-Q, Thach T-D, Nguyen C-L, Banh K-S, Le V-D, Nguyen L-P (2021) Biosynthesis of metallic nanoparticles from waste Passiflora edulis peels for their antibacterial effect and catalytic activity. Arabian J Chem 14(4):103096
29. Chau TP, Veeraragavan GR, Narayanan M, Chinnathambi A, Alharbi SA, Subramani B, Brindhadevi K, Pimpimon T, Pikulkaew S (2022) Green synthesis of zirconium nanoparticles using Punica granatum (pomegranate) peel extract and their antimicrobial and antioxidant potency. Environ Res 209:112771
30. Abdullah F, Bakar NA, Bakar MA (2020) Low temperature biosynthesis of crystalline zinc oxide nanoparticles from Musa acuminata peel extract for visible-light degradation of methylene blue. Optik 206:164279
31. Khammar Z, Sadeghi E, Raesi S, Mohammadi R, Dadvar A, Rouhi M (2022) Optimization of biosynthesis of stabilized silver nanoparticles using bitter orange peel by-products and glycerol. Biocatal Agric Biotechnol 43:102425
32. Mulla NA, Otari SV, Bohara RA, Yadav HM, Pawar SH (2020) Rapid and size-controlled biosynthesis of cytocompatible selenium nanoparticles by Azadirachta indica leaves extract for antibacterial activity. Mater Lett 264:127353
33. Saad AM, El-Saadony MT, El-Tahan AM, Sayed S, Moustafa MA, Taha AE, Taha TF, Ramadan MM (2021) Polyphenolic extracts from pomegranate and watermelon wastes as substrate to fabricate sustainable silver nanoparticles with larvicidal effect against Spodoptera littoralis. Saudi J Biol Sci 28(10):5674–5683
34. N.C.f.C.L. Standards (2002) Reference method for broth dilution antifungal susceptibility testing of yeasts, National Committee for Clinical Laboratory Standards Wayne, PA
35. Valgas C, Souza SMD, Smânia E, Smânia A (2007) Screening methods to determine antibacterial activity of natural products. Braz J Microbiol 38:369–380
36. Van de Loosdrecht A, Beelen R, Ossenkoppele G, Broekhoven M, Langenhuijsen M (1994) A tetrazolium-based colorimetric MTT assay to quantitate human monocyte mediated cytotoxicity against leukemic cells from cell lines and patients with acute myeloid leukemia. J Immunol Methods 174(1–2):311–320
37. El Shafey AM (2020) Green synthesis of metal and metal oxide nanoparticles from plant leaf extracts and their applications: a review. Green Process Synth 9(1):304–339
38. Fahimirad S, Ajalloueian F, Ghorbanpour M (2019) Synthesis and therapeutic potential of silver nanomaterials derived from plant extracts. Ecotoxicol Environ Saf 168:260–278
39. Paiva-Santos AC, Herdade AM, Guerra C, Peixoto D, Pereira-Silva M, Zeinali M, Mascarenhas-Melo F, Paranhos A, Veiga F (2021) Plant-mediated green synthesis of metal-based nanoparticles for dermopharmaceutical and cosmetic applications. Int J Pharm 597:120311
40. Yilmaz MT, İspirli H, Taylan O, Dertli E (2021) A green nanobiosynthesis of selenium nanoparticles with Tarragon extract: structural, thermal, and antimicrobial characterization. LWT 141:110969
41. Aslam M, Abdullah AZ, Rafatullah M (2021) Recent development in the green synthesis of titanium dioxide nanoparticles using plant-based biomolecules for environmental and antimicrobial applications. J Ind Eng Chem 98:1–16
42. Singh J, Dutta T, Kim K-H, Rawat M, Samddar P, Kumar P (2018) 'Green' synthesis of metals and their oxide nanoparticles: applications for environmental remediation. J Nanobiotechnol 16(1):84
43. Sui M, Kunwar S, Pandey P, Lee J (2019) Strongly confined localized surface plasmon resonance (LSPR) bands of Pt, AgPt, AgAuPt nanoparticles. Sci Rep 9(1):1–14
44. Akhtar S, Ismail T, Fraternale D, Sestili P (2015) Pomegranate peel and peel extracts: chemistry and food features. Food Chem 174:417–425
45. Nasiriboroumand M, Montazer M, Barani H (2018) Preparation and characterization of biocompatible silver nanoparticles using pomegranate peel extract. J Photochem Photobiol B 179:98–104
46. Liu Y, Zhang Q, Xu M, Yuan H, Chen Y, Zhang J, Luo K, Zhang J, You B (2019) Novel and efficient synthesis of Ag-ZnO nanoparticles for the sunlight-induced photocatalytic degradation. Appl Surf Sci 476:632–640
47. Kelly KL, Coronado E, Zhao LL, Schatz GC (2003) The optical properties of metal nanoparticles: the influence of size, shape, and dielectric environment, ACS Publications
48. Prasad KS, Selvaraj K (2014) Biogenic synthesis of selenium nanoparticles and their effect on As (III)-induced toxicity on human lymphocytes. Biol Trace Elem Res 157(3):275–283
49. Lawrie A, Albanyan A, Cardigan R, Mackie I, Harrison P (2009) Microparticle sizing by dynamic light scattering in fresh-frozen plasma. Vox Sang 96(3):206–212
50. Monika P, Chandraprabha M, Hari Krishna R, Vittal M, Likhitha C, Pooja N, Chaudhary V (2022) Recent advances in pomegranate peel extract mediated nanoparticles for clinical and biomedical applications. Biotechnol Genet Eng Rev 1–29. https://doi.org/10.1080/02648725.2022.2122299
51. El-Batal AI, Abd Elkodous M, El-Sayyad GS, Al-Hazmi NE, Gobara M, Baraka A (2020) Gum Arabic polymer-stabilized and Gamma rays-assisted synthesis of bimetallic silver-gold nanoparticles: powerful antimicrobial and antibiofilm activities against pathogenic microbes isolated from diabetic foot patients. Int J Biol Macromol 165:169–186
52. Castro-Longoria E, Vilchis-Nestor AR, Avalos-Borja M (2011) Biosynthesis of silver, gold and bimetallic nanoparticles using the filamentous fungus Neurospora crassa. Colloids Surf B 83(1):42–48
53. Nissen M, Förster R, Wieduwilt T, Lorenz A, Jiang S, Hauswald W, Schmidt MA (2022) Nanoparticle tracking in single-antiresonant-element fiber for high-precision size distribution analysis of mono-and polydisperse samples. Small 18(38):2202024
54. Souza TG, Ciminelli VS, Mohallem NDS (2016) A comparison of TEM and DLS methods to characterize size distribution of ceramic nanoparticles. J Phys: Conference Series IOP Publishing, p 012039

55. Mohsin M, Jawad M, Yameen MA, Waseem A, Shah SH, Shaikh AJ (2020) An insight into the coating behavior of bimetallic silver and gold core-shell nanoparticles. Plasmonics
56. Zhan X, Zhang H, Hou H, Gao F, Wang L, Ou D, Li B, Xu L, Yang W (2023) Rationally designed Ta3N5/ZnO core-shell nanofibers for significantly boosts photocatalytic hydrogen production. Appl Surf Sci 611:155788
57. Habibipour R, Moradi-Haghgou L, Farmany A (2019) Green synthesis of AgNPs@ PPE and its Pseudomonas aeruginosa biofilm formation activity compared to pomegranate peel extract. Int J Nanomed, 2019(14):6891–6899. https://doi.org/10.2147/IJN.S209912
58 Jyoti K, Baunthiyal M, Singh A (2016) Characterization of silver nanoparticles synthesized using Urtica dioica Linn. leaves and their synergistic effects with antibiotics. J Radiat Res Appl Sci 9(3):217–227
59. Bigdeli F, Morsali A (2010) Synthesis ZnO nanoparticles from a new Zinc (II) coordination polymer precursor. Mater Lett 64(1):4–5
60. Poyraz S, Cerkez I, Huang TS, Liu Z, Kang L, Luo J, Zhang X (2014) One-step synthesis and characterization of polyaniline nanofiber/silver nanoparticle composite networks as antibacterial agents. ACS Appl Mater Interfaces 6(22):20025–20034
61. Belavi P, Chavan G, Naik L, Somashekar R, Kotnala R (2012) Structural, electrical and magnetic properties of cadmium substituted nickel–copper ferrites. Mater Chem Phys 132(1):138–144
62. Pal K, Elkodous MA, Mohan MM (2018) CdS nanowires encapsulated liquid crystal in-plane switching of LCD device. J Mater Sci: Mater Electron 29(12):10301–10310
63. Mohammed G, Al-Jassani M, Hameed I (2016) Antibacterial, antifungal activity and chemical analysis of Punica grantanum (pomegranate peel) using GCMS and FTIR spectroscopy. Int J Pharmacogn Phytochem Res 8(3):480–494
64. Pereira PHF, Oliveira TÍS, Rosa MF, Cavalcante FL, Moates GK, Wellner N, Waldron KW, Azeredo HM (2016) Pectin extraction from pomegranate peels with citric acid. Int J Biol Macromol 88:373–379
65. Oliveira RN, Mancini MC, Oliveira FCSd, Passos TM, Quilty B, Thiré RMdSM, McGuinness GB (2016) FTIR analysis and quantification of phenols and flavonoids of five commercially available plants extracts used in wound healing. Matéria (Rio de Janeiro) 21:767–779
66. Al-Qahtani KM (2015) Heavy metals removal from polluted water by activated carbon prepared from pomegranate peel. Am Eurasian J Agric Environ Sci 15(4):595–602
67. Zaharia A, Muşat V, Ghisman VP, Baroiu N (2016) Antimicrobial hybrid biocompatible materials based on acrylic copolymers modified with (Ag) ZnO/chitosan composite nanoparticles. Eur Polymer J 84:550–564
68. Alrebdi TA, Ahmed HA, Alrefaee SH, Pashameah RA, Toghan A, Mostafa AM, Alkallas FH, Rezk RA (2022) Enhanced adsorption removal of phosphate from water by Ag-doped PVA-NiO nanocomposite prepared by pulsed laser ablation method. J Market Res 20:4356–4364
69. El-Batal AI, Balabel NM, Attia MS, El-Sayyad GS (2020) Antibacterial and antibiofilm potential of mono-dispersed stable copper oxide nanoparticles-streptomycin nano-drug: implications for some potato plant bacterial pathogen treatment. J Clust Sci 31:1021–1040. https://doi.org/10.1007/s10876-019-01707-4
70. Ibănescu M, Muşat V, Textor T, Badilita V, Mahltig B (2014) Photocatalytic and antimicrobial Ag/ZnO nanocomposites for functionalization of textile fabrics. J Alloy Compd 610:244–249
71. Nagaraju G, Prashanth S, Shastri M, Yathish K, Anupama C, Rangappa D (2017) Electrochemical heavy metal detection, photocatalytic, photoluminescence, biodiesel production and antibacterial activities of Ag–ZnO nanomaterial. Mater Res Bull 94:54–63
72. Wei Y, Chong YB, Du H, Kong J, He C (2018) Loose yarn of Ag-ZnO-PAN/ITO hybrid nanofibres: preparation, characterization and antibacterial evaluation. Mater Des 139:153–161
73. Zaheer Z, Albukhari SM (2020) Fabrication of zinc/silver binary nanoparticles, their enhanced microbial and adsorbing properties. Arab J Chem 13(11):7921–7938
74. Baptista PV, McCusker MP, Carvalho A, Ferreira DA, Mohan NM, Martins M, Fernandes AR (2018) Nano-strategies to fight multidrug resistant bacteria—"a battle of the titans." Front Microbiol 9:1441
75. Arora N, Thangavelu K, Karanikolos GN (2020) Bimetallic nanoparticles for antimicrobial applications. Front Chem 8:412
76. Zhang L, Jiang Y, Ding Y, Povey M, York D (2007) Investigation into the antibacterial behaviour of suspensions of ZnO nanoparticles (ZnO nanofluids). J Nanopart Res 9(3):479–489
77. Diem PNH, Phuong TNM, Hien NQ, Quang DT, Hoa TT, Cuong ND (2020) Silver, gold, and silver-gold bimetallic nanoparticle-decorated dextran: facile synthesis and versatile tunability on the antimicrobial activity. J Nanomater 2020:1–11
78. Gutiérrez JA, Caballero S, Díaz LA, Guerrero MA, Ruiz J, Ortiz CC (2018) High Antifungal activity against Candida species of monometallic and bimetallic nanoparticles synthesized in nanoreactors. ACS Biomater Sci Eng 4(2):647–653
79. Ioset J-R, Brun R, Wenzler T, Kaiser M, Yardley V (2009) Drug screening for kinetoplastids diseases. A Train Manual Screen in neglected diseases.DNDi and Pan-Asian Screening Network, 1–74. https://dndi.org/scientific-articles/2009/drug-screening-for-kinetoplastid-diseases-a-training-manual-for-screening-in-neglected-diseases/
80. Ambujakshi N, Raveesha H, Manohara S, Dhananjaya N, Pratibha S, Shivakumara C (2019) Chonemorpha grandiflora extract mediated synthesis of Ag-ZnO nanoparticles for its anticancer, electrical and dielectric applications. Mater Res Express 6(9):095068
81 Elsayed KA, Alomari M, Drmosh QA, Alheshibri M, Al Baroot A, Kayed TS, Manda AA, Al-Alotaibi AL (2022) Fabrication of ZnO-Ag bimetallic nanoparticles by laser ablation for anticancer activity. Alex Eng J 61(2):1449–1457
82. Pandiyan N, Murugesan B, Arumugam M, Sonamuthu J, Samayanan S, Mahalingam S (2019) Ionic liquid - a greener templating agent with Justicia adhatoda plant extract assisted green synthesis of morphologically improved Ag-Au/ZnO nanostructure and it's antibacterial and anticancer activities. J Photochem Photobiol, B 198:111559